Chapter 7
Evolution of Polarization Singularities of Two Monochromatic Beams in Their Collinear Interaction in an Isotropic Medium with Spatial Dispersion of Cubic Nonlinearity

Vladimir Makarov

7.1 Introduction

I am going talk about the results [1] obtained by our team in the investigation of the appearance of polarization singularities and its interaction in nonlinear optics problems, more specifically, about the interaction of two monochromatic beams with defined structure containing the polarization singularities in the case of their collinear propagation in an isotropic gyrotropic medium with cubic nonlinearity. The simplest example of an isotropic chiral medium is an isotropic solution of large bioorganic molecules, which differ from their mirror images (Fig. 7.1), in a word, chiral molecules.

Inhomogeneously polarized monochromatic electromagnetic fields may contain lines of circular polarization also known as lines of polarization singularity (*C*-lines) [2]. In paraxial beams, the intersections of the *C*-lines with the plane transversal to the propagation direction are treated as *C*-points. The behavior of the *C*-points in various linear media is frequently studied in scientific works (see, for example, [3–6]). Methods for the description of the *C*-point dynamics [7] and their experimental detection [8] have been developed; the statistics of the *C*-points in random light fields have also been studied [9–11]. In addition, there are certain applications of polarization singularities in problems of biology [12].

V. Makarov (✉)
Faculty of Physics and International Laser Center,
Lomonosov Moscow State University, Leninskie Gory 1,
Moscow 119991, Russia
e-mail: vamakarov@phys.msu.ru

K. Yamanouchi (ed.), *Progress in Photon Science*, Springer Series in Chemical Physics 115, DOI 10.1007/978-3-319-52431-3_7

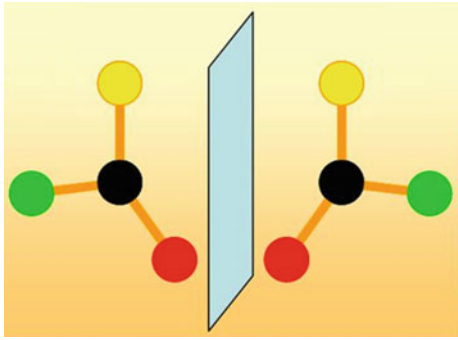

Fig. 7.1 Chiral molecule

The classification scheme for the *C*-points was first proposed in [2], based on the analogous scheme for the degenerate points of the two-dimensional symmetric tensor field. In connection with this, they are assumed to vary among three basic types of *C*-points: the *lemon*, the *monstar,* and the *star*. The most important characteristic of the *C*-point is its topological index, which is the number of full rotations of the polarization ellipse on a counterclockwise loop around the *C*-point. The lemon and the monstar points have a topological index 1/2. This is because the polarization ellipse rotates at 180° on a counterclockwise loop around the *C*-point. The difference between these two types is in the orientation of the polarization ellipses in the vicinity of the *C*-point [13]. The star *C*-point has a topological index −1/2 (see Fig. 7.2).

C-points can also be treated as phase singularities of the circularly polarized components of the electromagnetic radiation [13]. The complex amplitude of one of the circularly polarized components of the field becomes zero at the *C*-point, and

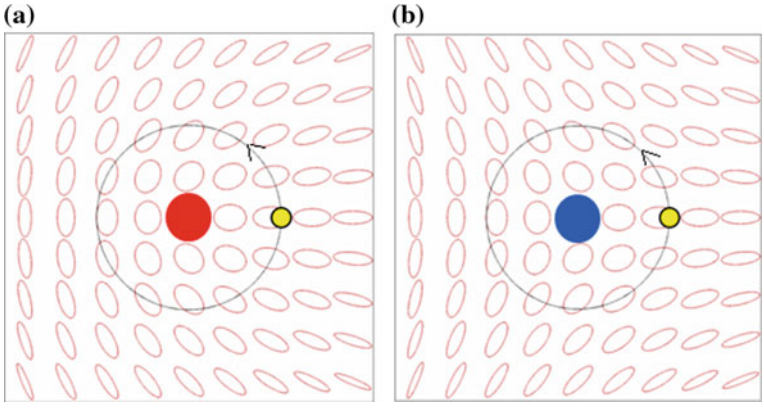

Fig. 7.2 **a** The lemon and the monstar *C*-points (*red circle*) with topological index ½. The polarization ellipse rotates 180° on a counterclockwise loop around the *C*-point and. **b** The star *C*-point (*blue circle*) with topological index −½. The polarization ellipse rotates 180° on a clockwise loop around the *C*-point

the phase of this component becomes indefinite. The points of the phase singularities are also known as "optical vortices". There are a number of fundamental theoretical works [14–16] devoted to the linear interaction of the beams containing phase singularities with various structures, and the results of these works can be generalized for the case of the interacting beams with *C*-points.

Due to the features accompanying the formation of polarization singularities in nonlinear optical processes and their subsequent evolution in a nonlinear medium, there are countless resource-consuming methods for accounting for the polarization evolution in the process of wave propagation. However, such studies could be especially interesting. Formation of polarization singularities is possible due to the three-wave mixing in a nonlocal nonlinear medium, even in the case of uniformly polarized incident beams [17–20]. Moreover, numerical investigations have shown that the nonlocality of nonlinear medium plays the key role in the stabilization of the propagation of singular beams of a specific type [21–23]. Interest in the processes accompanying the filamentation of singular beams also increases [24, 25].

The aim of this work is the investigation of the interaction of two monochromatic beams with defined structure containing the polarization singularities in the case of their collinear propagation in an isotropic gyrotropic medium with cubic nonlinearity.

7.2 Theory

The propagation of the light beam in an isotropic gyrotropic medium with spatial dispersion of cubic nonlinearity can be described in terms of the following system of nonlinear equations [26, 27]:

$$\frac{\partial A_{\pm}}{\partial z} + \frac{i}{2k}\Delta_{\perp}A_{\pm} + i\Big[\mp\rho_0 + (\sigma_1/2 \mp \rho_1)|A_{\pm}|^2 + (\sigma_1/2 + \sigma_2)|A_{\mp}|^2\Big]A_{\pm} = 0 \tag{7.1}$$

for the slowly varying envelopes $A_{\pm}(z, x, y) = A_x \pm iA_y$ of the circularly polarized components of the light field. Here $\Delta_{\perp}$ is a Laplace operator in transversal coordinates, ω is the frequency of the wave propagating in the z-direction, and k is its wave number. The parameters $\sigma_1 = 4\pi\omega^2\chi_{xyxy}/(kc^2)$ and $\sigma_2 = 2\pi\omega^2\chi_{xxyy}/(kc^2)$ are proportional to the components of the fourth-rank tensor of local cubic optical response $\hat{\chi}^{(3)}(\omega; -\omega, \omega, \omega)$, which possesses a permutation symmetry for the last two indices. Parameter $\rho_{0,1} = 2\pi\omega^2\gamma_{0,1}/c^2$ is proportional to the pseudoscalar constants of linear and nonlinear gyration γ_0 and γ_1, which are the nonzero components of nonlocal linear $\hat{\gamma}^{(1)}$ and nonlinear (cubic) $\hat{\gamma}^{(3)}$ optical susceptibilities, contributing $\hat{\gamma}^{(1)}\vec{\nabla}\vec{E}$ and $\hat{\gamma}^{(3)}\vec{E}\vec{E}\vec{\nabla}\vec{E}$ to the polarization of the medium [28–30]. Further we assume that all of these medium parameters have real values.

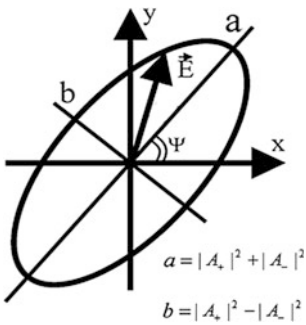

Fig. 7.3 Polarization ellipse parameters

The propagating radiation can be fully characterized by the intensity $I(x,y,z) = \left(|A_+|^2 + |A_-|^2\right)/2$, the ellipticity degree of the polarization ellipse $M(x,y,z) = \left(|A_+|^2 - |A_-|^2\right)/2I$, and the angle of orientation of the polarization ellipse $\Psi(x,y,z) = \mathrm{Arg}\left(A_+ A_-^*\right)/2$ (see Fig. 7.3). Let us consider two coherent monochromatic beams falling along the z-axis onto the medium surface $z = 0$ normally. We assume the beams each have the following structure: the right-handed circularly polarized component has a Gaussian profile, while the left-handed circularly polarized one has a Laguerre–Gaussian profile. Their centers are located on the x-axis at a distance, each at $d/2$ from the zero point. Right-handed circularly polarized components of these beams at $z = 0$ are given by the following expressions:

$$A_{+1}(x,y) = E_0 \exp\left(-\frac{(x+d/2)^2 + y^2}{w^2}\right), \tag{7.2}$$

$$A_{+2}(x,y) = E_0 \exp(i\theta) \exp\left(-\frac{(x-d/2)^2 + y^2}{w^2}\right), \tag{7.3}$$

and the left-handed circularly polarized ones are given as:

$$A_{-1}(x,y) = hE_0\left(\frac{x+d/2 \mp iy}{w}\right) \exp\left(-\frac{(x+d/2)^2 + y^2}{w^2}\right), \tag{7.4}$$

$$A_{-2}(x,y) = hE_0 \exp(i\theta)\left(\frac{x-d/2 \mp iy}{w}\right) \exp\left(-\frac{(x-d/2)^2 + y^2}{w^2}\right). \tag{7.5}$$

Here, $\exp(i\theta)$ determines the phase shift between the beams, E_0 is the amplitude, and h is a real-value coefficient. When $d >> w$, both beams have radial symmetric intensity distributions and C-points in their centers $(-d/2,\ 0,\ 0)$ and $(d/2,\ 0,\ 0)$.

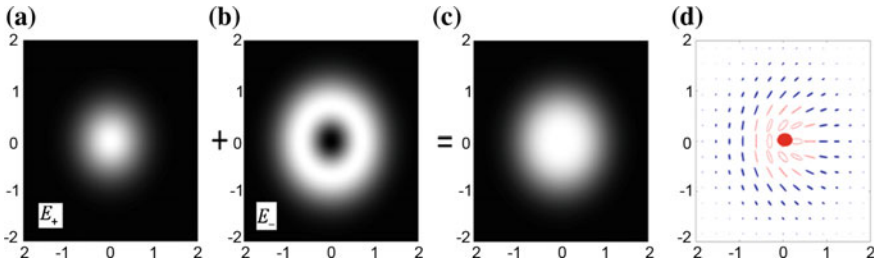

Fig. 7.4 The intensity distribution in *right-handed circularly* polarized component with Gaussian profile (**a**) and in the *left-handed circularly* polarized one with Laguerre–Gaussian profile (**b**), the intensity (**c**), and polarization (**d**) distributions in the resulting beam. The *right-handed circularly* polarized *C*-point (*red circle*) with topological index ½ is located at the center of the beam ($x = 0$; $y = 0$)

The radiation is right-handed circularly polarized in these *C*-points. If there is a "−" in the expression (7.4) and (7.5) before the imaginary unit, then the topological index of the *C*-point is 1/2, and, if there is a "+" in these equations, then the topological index is −1/2. In the case of positive topological index, the *C*-point given by the expressions above will have a "lemon" morphologic type (see Fig. 7.4), and, in the case of negative topological index, it will be a "star". Within the framework of our study, we do not pay attention to the transformation of lemon to monstar and vice versa, neither do we make any difference between these two morphological types with positive topological charge. We limit ourselves to the investigation of topological charge evolution, nucleation, and annihilation of the *C*-points with opposite topological charges. Figure 7.4d shows typical transversal polarization distribution in one of the incident beams in the case of the topological index 1/2. Each ellipse in the figure shows the polarization ellipse in the corresponding point of the beam cross section with the same parameter (ellipticity degree, angle of orientation). The sum of squares of axes of the ellipse is proportional to the intensity of light at the given point. Filled ellipses correspond to the left-handed circularly polarized components, and the open ellipses correspond to the right-handed circularly polarized radiation.

The system of equations (7.1) is symmetrical to the simultaneous change of $E_\pm$ to $E_\mp$ and $\rho_{0,1}$ to $-\rho_{0,1}$. In this case, the indices of the *C*-points of the incident beams, the ellipticity degrees, and the orientation angles of the polarization ellipses in them change their sign to the opposite in each point of space. Moreover, the simultaneous change of the topological indices of the *C*-points in the incident beams, which can be achieved by the change of "∓" to "±" in (7.4) and (7.5), is equivalent to the reversion of the *y*-axis, i.e., the spatial distribution of the electromagnetic field is mirror-reflected from the plane $y = 0$. Owing to the medium symmetry, the trajectories of the singularities (the *C*-lines) will be reflected relative to the plane $y = 0$. The effect of linear gyration ($\rho_0 \neq 0$) causes the rotation of the polarization ellipses in each point in the transversal plane of the propagating field for any value of *z*. The angle of rotation is proportional to the propagation

coordinate z and does not depend on the transversal coordinates. Thus, in this article, we do not take into account the linear gyration, focusing primarily on non-linear effects.

It is important to remark that the *C*-points with the opposite handedness of the polarization rotation do not interact in a linear medium. Thus, we can limit ourselves to the consideration of incident beams with right-handed circular polarization in both *C*-points with equal or opposite topological indices. In these two cases, the equation system (7.1) with boundary conditions (7.2)–(7.5) was solved numerically for various values of the incident radiation and nonlinear medium. Then the polarization distributions, shown in Fig. 7.4 in xy plane for various z values, were analyzed. The positions of *C*-points in these polarization distributions were found as points where the value of the polarization ellipse orientation angle Ψ was undefined. Afterwards, the topological indices of the *C*-points were found by the polarization distribution in their vicinity, and the *C*-lines were built.

It follows from (7.1) that, in a linear medium ($\sigma_{1,2} = 0$, $\rho_1 = 0$), the circularly polarized components of the light field $A_{\pm}$ with opposite handedness do not interact with each other. For any z, the right-handed circularly polarized component is a superposition of two non-coaxial Gaussian beams that spread during the propagation. As the result of merging two Gaussian beams, an intensity maximum is formed between their centers, which we call the "central maximum" hereafter. The left-handed circularly polarized component is a superposition of two non-coaxial Laguerre–Gaussian beams, and its shape experiences more sophisticated changes during the propagation. Each beam loses its cylindrical symmetry. There appear spots at their "rings", where the formation of the intensity maxima take place, which further we call them the "lateral maxima". With the increase of z, these maxima move away from the center. As a result, three intensity maxima appear in the transversal section of superimposed propagating beams.

In the case of the equal sign of the topological charges of the *C*-points in the incident beams, the interference of the beams at $z = 0$ yields one or three *C*-points, depending on d, h, and θ, instead of two. The sum of the topological charges of all of the *C*-points in both cases is equal to +1/2 or −1/2, depending on the sign of the topological charge of the separate *C*-points. The appearance and the propagation of a sole *C*-point is not of a major factor, so, therefore, we consider the situation in which three *C*-points arise at the border of the medium. The third *C*-point, which appears between two initially existing *C*-points, has the topological charge with the sign opposite to that of the initial *C*-points. If $h = 1$, its coordinates are $x_c = 0$, $y_c = -0.5d \cdot \mathrm{tg}\,(\theta/2)$, and they do not change with the propagation when z increases. After traversing a distance of $\tilde{z} = (d^2(1 + \cos\theta)^{-1} - 1)^{1/2}$, a dynamic inversion of its topological charge occurs, first described in [14]: the central *C*-point "exchanges" its topological charge with one of the other two *C*-points (Fig. 7.5a). In other words, two *C*-points with opposite topological charges annihilate, and afterwards another pair of the "oppositely charged" *C*-points appears immediately. Figure 7.5b shows the polarization distribution in the transversal plane for $z = 2L_d$,

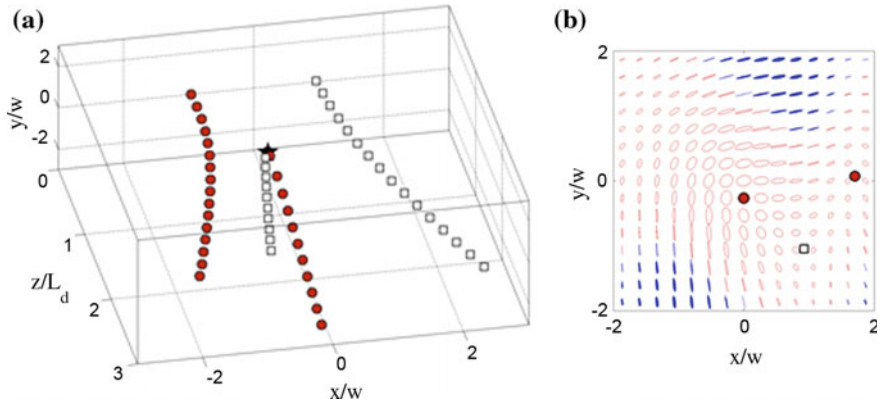

Fig. 7.5 The trajectories of the *C*-points in a linear medium in the case of equal signs of the topological indices of the incident beams (**a**) and the transversal polarization distribution in the propagating light at $z/L_d = 2$ (**b**) The parameters of the incident beams are the following: $d = 2$, $h = 1$, $\theta = 30°$. *Circles* indicate the *C*-line in (**a**) (*C*-points in (**b**)) with +1/2-topological index, and *squares* indicate the *C*-line in (**a**) (C-points in (**b**)) with −1/2-topological index. The point of pairwise creation/annihilation of the *C*-points is designated by a star ($\tilde{z}/L_d \approx 1.07$)

where $L_d = kw^2/2$.The circles indicate the *C*-points with the topological charge +1/2, and a square indicates the *C*-point with a topological charge of −1/2.

In the case of opposite topological charges of the *C*-points in the incident beams, there can be two or four *C*-points at the border of the medium as a result of their interference, depending on d, h, and θ. If four *C*-points appear there, two "additional" *C*-points have opposite topological charges, so that the sum of topological charges of all of the *C*-points is equal to zero. We will consider only the case when there are two *C*-points, located in the centers of incident beams. If $\theta = 0$, then for any value of $z = z_1$ the light in each point of the straight line $\{x = 0; z = z_1\}$ is right-handed circularly polarized, because the left-handed circularly polarized Laguerre–Gaussian components suppress each other at this line. In this case, the abovementioned straight line is a symmetry axis for the intensity distribution in the transversal plane.

Let us consider the case when there is only one pair of *C*-points with the opposite topological charges at the border of the medium. If $\theta \neq 0$ and $d > \sqrt{2}$, then, after traversing some distance, an additional pair of *C*-points with opposite topological charges is nucleated as shown in Fig. 7.6a. The corresponding transversal polarization distribution for $z = 2L_d$ is shown in Fig. 7.6b. If the phase shift θ between the initial beams exceeds a certain critical value $\theta_{cr}(d)$, then one of the "new" *C*-points will subsequently be annihilated with one of the "old" *C*-points having the opposite topological charge (Fig. 7.6c). The transversal polarization distribution at $z = 2L_d$ for this case is shown in Fig. 7.6d. The dependence $\theta_{\mathrm{cr}}(d)$ is monotone (Fig. 7.7).

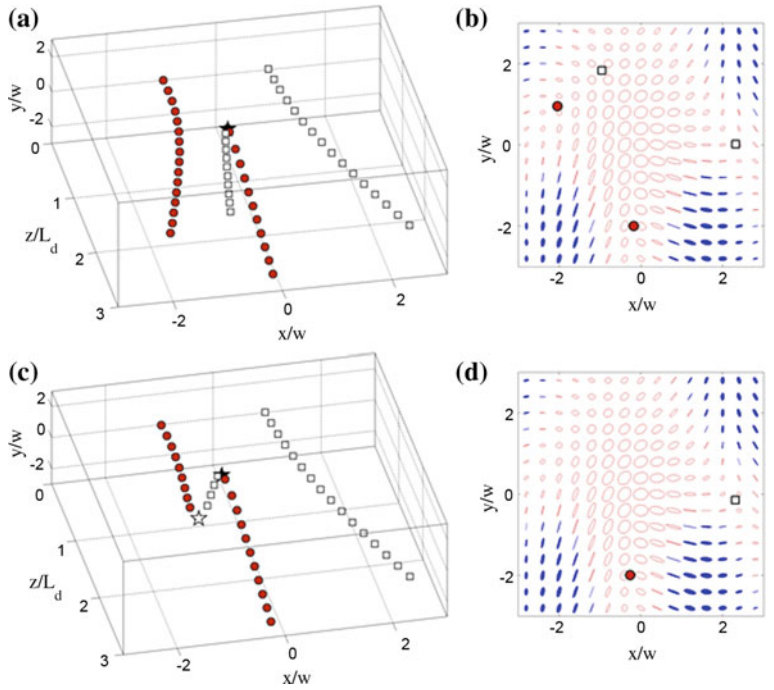

Fig. 7.6 The processes of the nucleation and the annihilation of the *C*-points (**a**, **c**) and the transversal polarization distributions at $z = 3L_d$ (**b**, **d**). Here $\theta = 20°$ in (**a**, **b**), and $\theta = 30°$ in (**c**, **d**). The topological charges of the C-points in the initial (separate) beams are opposite, $d = 2$, $h = 1$. The critical phase shift for this case is $\theta_{cr} \approx 24°$. *Circles* indicate the *C*-points with positive topological charge, and *squares* indicate those with the negative topological charge. Pairwise creation of the *C*-points is indicated by empty stars in (**a**) and (**c**), and pairwise annihilation is indicated by a filled star in (**c**)

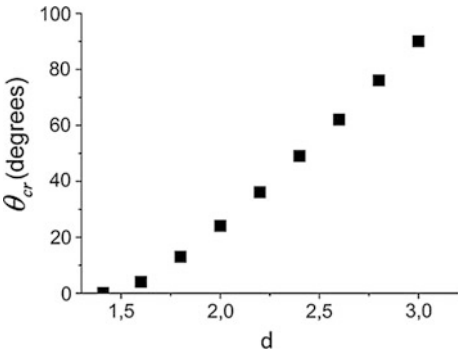

Fig. 7.7 Dependence of θ_{cr} on the distance between the centers of the incident beams d

In a nonlinear medium, the features of the interaction of the polarization singularities is determined by the parameters d/w, h, θ, σ_2/σ_1, ρ_1/σ_1 and the so-called dimensionless power $P = \sigma_1 L_d E_0^2$, which can easily be adjusted in the experiment. Our numerical investigations have shown its predominant influence on the features accompanying the propagation of the *C*-points. With the growth of P, these features take place at a smaller value of the nonlinear susceptibility of the medium, or at smaller distances traversed in a medium.

The coefficients $\sigma_1/2 \pm \rho_1$ in (7.1) are responsible for the self-action of the each circularly polarized component. In the case of the equal topological charges of the *C*-points in the initial beams, this self-action promotes the amplification of the central and lateral intensity maxima and their stability during the propagation. If $\sigma_1/2 + \sigma_2 > 0$, the circularly polarized components $A_\pm$ are focused on each other due to the nonlinear cross-interaction. In this case, each of the lateral maxima will be attracted to the corresponding central maxima with the opposite handedness of the polarization. In the case of significant focusing nonlinearity, the central spots of the Gaussian components do not merge, but propagate separately instead. As a result, there appear not three, but only two intense peaks in the transversal section of the propagating light, and their polarization is determined by the value of h. If $h \approx 1$, the polarization is almost linear. The intensity of light in the vicinity of each of the *C*-points, where the radiation is right-handed circularly polarized, tends to zero, since the power of this circularly polarized component is attracted by the component with the opposite rotation, that is the right-handed circularly polarized Gaussian is attracted by the left-handed circularly polarized Laguerre–Gaussian component. If $\sigma_1/2 + \sigma_2 < 0$, then the intensity maxima with opposite handedness of the polarization rotation defocuses on each other and tend to occupy areas in the beam cross section, which do not overlap. The polarization and the intensity distributions in this case become similar to those shown in Figs. 7.5 and 7.6 for approximately the same parameters of the incident beams. The maxima of the intensity maintain their shapes during the propagation owing to the nonlinear self-action and its contrasts. The larger one is the absolute value of the negative quantity σ_2/σ_1; the stronger one is the difference between the polarization state of this maximum and the linear polarization state.

Let us consider now the incidence of two beams with equal topological charges of the singularities onto the nonlinear medium. For any value of $\sigma_1/2 + \sigma_2$, the central *C*-point, originating in this case from the interference, does not move straight along the z-axis, as it does in a linear medium (Fig. 7.5a), and the dynamic inversion of its topological charge does not occur. Instead, two separate events of pairwise creation and annihilation of the *C*-points in a nonlinear medium take place (Fig. 7.8). Depending on the sign of the $\sigma_1/2 + \sigma_2$, the sequence of these two events can be different. Figure 7.9a, b show the dependence of the nucleation/annihilation distance on the dimensionless power parameter. As can be seen, the growth of P results in the increase of the z-coordinates of the *C*-points' nucleation/annihilation processes for $\sigma_1/2 + \sigma_2 > 0$ and in the decrease of these characteristic coordinates in the case of $\sigma_1/2 + \sigma_2 < 0$.

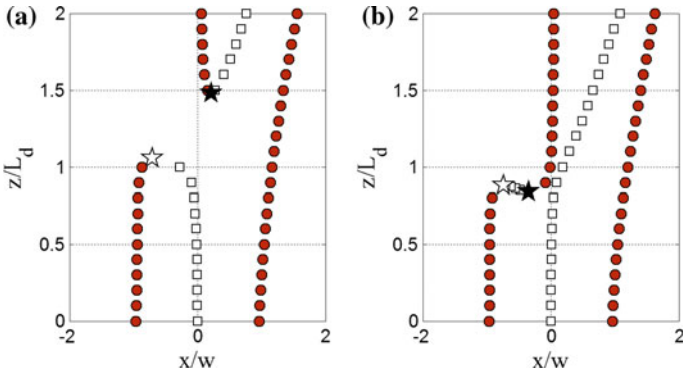

Fig. 7.8 *C*-lines in a nonlinear medium for $P = 1$, $\sigma_2/\sigma_1 = 0.5$, $\sigma_2/\sigma_1 = 0.5$, $\rho_1/\sigma_1 = 0$ (**a**) and $P = 2$, $\sigma_2/\sigma_1 = -0.8$, $\rho_1/\sigma_1 = 0$ (**b**). The parameters of the incident beams are $d = 2$, $\theta = 30^\circ$ and $h = 1$. *Circles* designate the *C*-lines with the topological charge 1/2, while *squares* designate ones with the topological charge −1/2. Pairwise creation of the *C*-points is indicated by *filled stars* and pairwise annihilation is indicated by empty ones

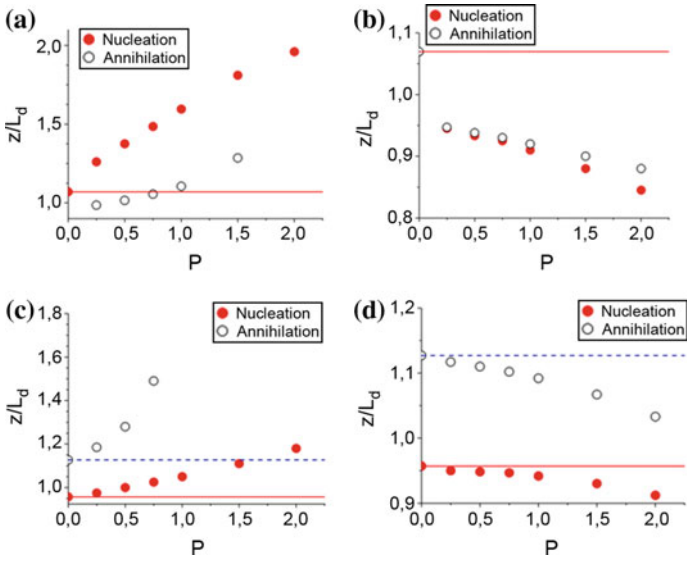

Fig. 7.9 The dependence of the distance from the border of the medium, where the nucleation/annihilation of two *C*-points takes place, on the dimensionless power parameter. *Filled circles* correspond to the nucleation and empty ones to annihilation. **a–b** equal topological charges of the initial singularities, $\theta = 30^\circ$. **c–d** opposite topological charges of the initial singularities, $\theta = 40^\circ$. (**a**, **c**) $\sigma_2/\sigma_1 = 0.5$, (**b**, **d**) $\sigma_2/\sigma_1 = -0.8$. Other parameters: $d = 2$, $h = 1$ and $\rho_1/\sigma_1 = 0$

In the case of the incident beams with the opposite topological charges of the polarization singularities, the trajectories of the *C*-points are similar to those as shown in Fig. 7.6. If we assume that the phase shift θ is greater than θ_{cr}, the pairwise annihilation of *C*-points is observed at certain $z = z^*$ in a linear medium (see Fig. 7.6c). If $\sigma_1/2 + \sigma_2 > 0$, the increase in the dimensionless power results in the increase in the annihilation coordinate z^* until it exceeds the limits of the calculation area. If $\sigma_1/2 + \sigma_2 < 0$, the annihilation occurs at smaller values in z^* with the increase of *P*. In other words, in the first case ($\sigma_1/2 + \sigma_2 > 0$), the evolution of the *C*-points proceeds more slowly, while, in the second case, it proceeds faster, compared to propagation in a linear medium. Such a behavior is common for small values of the dimensionless power ($P_1 \leq P \leq P_2$, where $P_1 \cong 1$, $P_2 \cong 3$). For larger values of *P*, the self-action of the circularly polarized components $A_\pm$ prevents the interaction of the incident beams and, therefore, the interaction of the *C*-points in them. The *z*-coordinate of the pairwise creation of *C*-points is affected by the change of the dimensionless power in a similar way as in Fig. 7.9c, d.

It can be seen from (7.1), that the spatial dispersion of the cubic nonlinearity enhances the self-action of one of the circularly polarized components of propagating light. In the case of equal topological charges of the incident beams, the presence of the spatial dispersion causes faster pairwise creation of the *C*-points with opposite topological charges at smaller distances as compared to the case when the spatial dispersion is absent ($\rho_1 = 0$). Corresponding transversal polarization distribution is shown in Fig. 7.10a. The growth of $|\rho_1|$ leads to the formation of strongly inhomogeneous polarization distribution (Fig. 7.10b). If $\sigma_1/2 + \sigma_2 < 0$, then the spatial dispersion of cubic nonlinearity affects the relative values of the intense peaks in the transversal intensity distribution of the propagating wave.

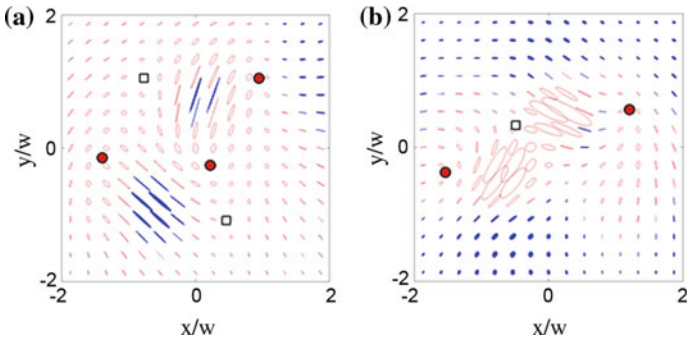

Fig. 7.10 The transversal polarization distribution at $z = 2L_d$ in the propagating wave in the case of equal topological charges of the singularities in the incident beams for the $d = 2$, $h = 1$, $\theta = 30°$, $P = 2$, $\sigma_2/\sigma_1 = 0.5$ and **a** $\rho_1/\sigma_1 = 0.4$, **b** $\rho_1/\sigma_1 = -0.4$

7.3 Conclusion

For the first time the interaction of two collinear specific-kind monochromatic beams with polarization singularities in the nonlinear isotropic gyrotropic medium was theoretically studied. The relations between the components of local and nonlocal cubic optical susceptibility tensors determine possible scenarios of the interaction of circularly polarized components of the light field. In the case of their mutual focusing, the spatial dispersion of cubic nonlinearity determines the polarization states of the intensity maxima in the propagating light. Otherwise, in the case of the defocusing cross-interaction of the circularly polarized components, the spatial dispersion of cubic nonlinearity directly affects the relative intensities of the peaks in the transversal intensity distribution.

The processes of pairwise creation and annihilation of the *C*-points with opposite topological charges in the bulk of the nonlinear medium were observed. The sum of the topological charges of all of the *C*-points in the transversal section of the propagating light remains constant as the z coordinate changes. The nonlinearity of the medium plays a key role in the scenario of the evolution of the *C*-points. In the case of the mutual focusing of the circularly polarized components of the light field, the increase in the intensity of the incident beams leads to the retardation of the interaction of the *C*-points. In the case of the mutual defocusing of the circularly polarized components of the propagating light, the greater the intensity of the incident beams becomes, the faster the processes of pairwise creation/annihilation proceed.

Acknowledgements We acknowledge financial support from the Russian Foundation for Basic Research (Grant No. 13-02-00324) and the support from a grant of the President of the Russian Federation for state support of leading scientific schools (Grant No. NSh-3796.2014.2). I am indeed grateful to Dr. I.A. Perezhogin and Dr. K.S Grigoriev for stimulating discussions with and invaluable help, some results of common work were observe in this report.

References

1. K.S. Grigoriev, V.A. Makarov, I.A. Perezhogin, J. Optics. **16**(105201), 8 (2014)
2. J.F. Nye, Proc. R. Soc. **389**, 279 (1983)
3. KYu. Bliokh, A. Niv, V. Kleiner, E. Hazman, Opt. Express **16**, 709 (2008)
4. F. Flossmann, U.T. Schwarz, M. Maier, M.R. Dennis, Phys. Rev. Lett. **95**, 253901 (2005)
5. M.V. Berry, M.R. Dennis, Proc. Royal. Soc. **459A**, 1261 (2003)
6. YuA Egorov, T.A. Fadeyeva, A.V.J. Volyar, Opt. A **6**, 217 (2004)
7. K. O'Holleran, F. Flossmann, M.R. Dennis, M.J.J. Padgett, Opt. A. Opt. **11**(094020) (2009)
8. O.V. Angelsky, I.I. Mokhun, A.I. Mokhun, M.S. Soskin, Phys. Rev. E **65**, 036602 (2002)
9. M.V. Berry, M.R. Dennis, Proc. Royal. Soc. **457A**, 141 (2001)
10. G.V. Bogatyryova, K.V. Felde, P.V. Polyanskii, M.S. Soskin, Opt. Spectrosc. **97**, 833 (2004)
11. Y.F. Chen, T.H. Lu, K.F. Huang, Phys. Rev. Lett. **96**, 033901 (2006)
12. O.V. Angelsky, A.G. Ushenko, YuA Ushenko, E.G. Ushenko, J. Phys. D **39**, 3547 (2006)
13. M.R. Dennis, Opt. Lett. **33**, 2572 (2008)

14. D. Rozas, C.T. Law, G.A. Jr. Swartzlander, J. Opt. Soc. Amer. B. **14**, 3054–3065 (1997)
15. V. Pyragaite, A. Stabinis, Opt. Comm. **220**, 247 (2003)
16. S. Orlov, A. Stabinis, Opt. Comm. **226**, 97 (2003)
17. V.A. Makarov, I.A. Perezhogin, N.N. Potravkin, Quantum Electron. **41**, 149 (2011)
18. K.S. Grigoriev, V.A. Makarov, I.A. Perezhogin, N.N. Potravkin, Quantum Electron. **41**, 993 (2011)
19. I.A. Perezhogin, V.A. Makarov, J. Opt. A **11**, 074008 (2009)
20. V.A. Makarov, I.A. Perezhogin, N. N. Portavkin. J. Opt. **14**, 055202 (2012)
21. A.S. Desyatnikov, YuS Kivshar, Prog. Opt. **47**, 291 (2005)
22. S. Lopez-Aguayo, J.C. Gutiérrez-Vega, Opt. Express **15**, 18326 (2007)
23. S. Lopez-Aguayo, A.S. Desyatnikov, Yu. S. Kivshar Opt. Express **14**, 7903 (2006)
24. Georgi Maleshkov et al., J. Opt. **13**, 064015 (2011)
25. O. Khasanov, T. Smirnova, O. Fedotova, G. Rusetsky, O. Romanov, App. Opt. **51**, 198 (2012)
26. A.A. Golubkov, V.A. Makarov, Radiophysics and Quantum. Electronics **31**, 1042 (1988)
27. A.A. Golubkov, V.A. Makarov, I.A. Perezhogin, Mosc. Univ. Phys. Bull. **64**, 54 (2009)
28. S.A. Akhmanov, V.I. Zharikov, JETP Lett. **6**, 137 (1967)
29. S.A. Akhmanov, G.A. Lyakhov, V.A. Makarov, V.I. Zharikov, Optica Acta **29**, 1359 (1982)
30. A.A. Golubkov, V.A. Makarov, J. Modern Optics **37**, 1531 (1990)